AD-A115 069 ELECTRO MAGNETIC APPLICATIONS INC GOLDEN CO F/G 1/3
COUPLING OF LIGHTNING STROKE CURRENT TO AIRCRAFT BALANCED TWIST--ETC(U)
MAR 79 R B COOK, R A PERALA N00019-79-C-0584

UNCLASSIFIED NL

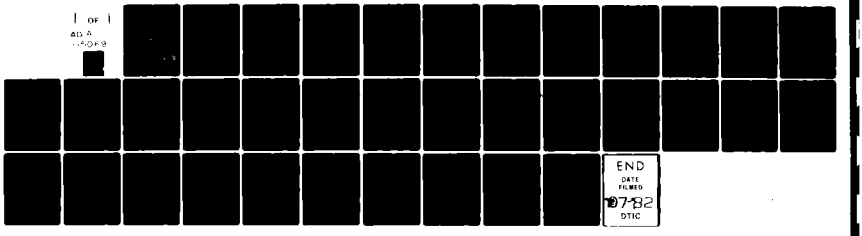

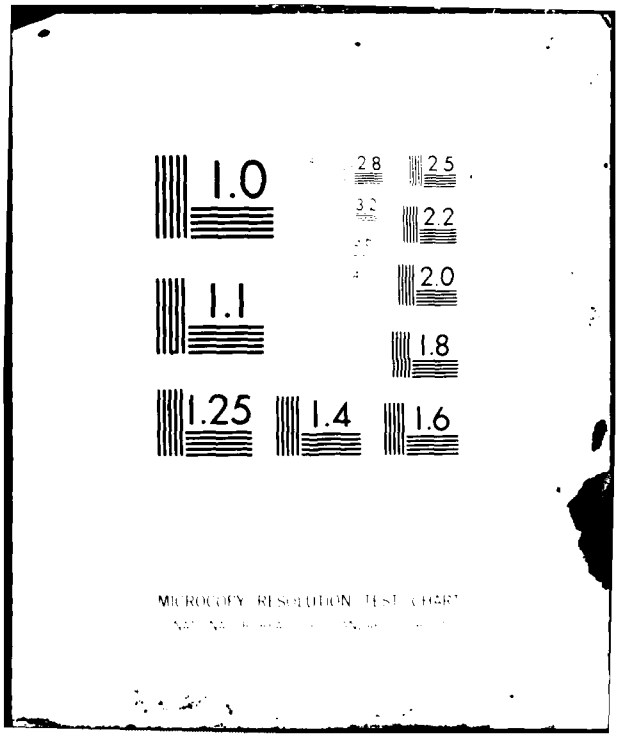
1.0
2.8
2.5
2.2
2.0
1.1
1.8
1.25
1.4
1.6
MICROCOPY RESOLUTION TEST CHART

(1)

AIR-518-5

COUPLING OF LIGHTNING STROKE CURRENT TO AIRCRAFT BALANCED TWISTED SHIELDED PAIR CABLES

March 1979

Contract Number N0019-79-G-0584

NAVAL AIR SYSTEM COMMAND
U.S. DEPARTMENT OF THE NAVY

EMA ELECTRO MAGNETIC APPLICATIONS, INC.

P. O. Box 8
Golden, Colorado 80401

COUPLING OF LIGHTNING STROKE CURRENTS TO F-18 BALANCED TWISTED SHIELDED PAIR CABLES

by

R. B. Cook
R. A. Perala

March, 1979

Prepared For

Naval Air Systems Command
AIR-52026B
Washington, D. C., 20361

TABLE OF CONTENTS

LIST OF ILLUSTRATIONS

LIST OF TABLES

COUPLING OF LIGHTNING STROKE CURRENTS TO F-18 BALANCED TWISTED SHIELDED PAIR CABLES

CHAPTER 1

INTRODUCTION

The F-18 is the first military aircraft which makes extensive use of graphite epoxy composite materials. These materials are used on the wings, tail, horizontal stabilizer, and on various access doors and panels. Figure 1 illustrates the usage locations. The aircraft also uses fly-by-wire technology in all axes, although it has mechanical back-up in all axes except for yaw. The aircraft can land at an airfield on these backups alone, however, aircraft carrier landings may be somewhat more hazardous. In addition, the aircraft avionics make extensive use of low-level integrated circuit technology, including the flight control computer, the AYK-14.

In view of these facts, electromagnetic hazards assume a more important role in aircraft survivability, both to man-made and natural threats. In particular, the use of graphite epoxy composites implies a shielding effectiveness which is less than that obtained on metallic aircraft, because of the composite's smaller (by a factor of ~ 10^3) electrical conductivity and the problem associated with obtaining good electrical joints (composite/composite as well as metal/composite).

The scope of this investigation is not to investigate the susceptibility of the aircraft to all electromagnetic threats. Instead, one of the threats of greatest concern, an attached lightning stroke, is the subject of the investigation. In particular, the threat caused by a direct strike to the nose/tail is examined for the cables which route across access doors of composite/aluminum honeycomb construction with special treatment of the edges to avoid corrosion. There is concern that, because of the proximity

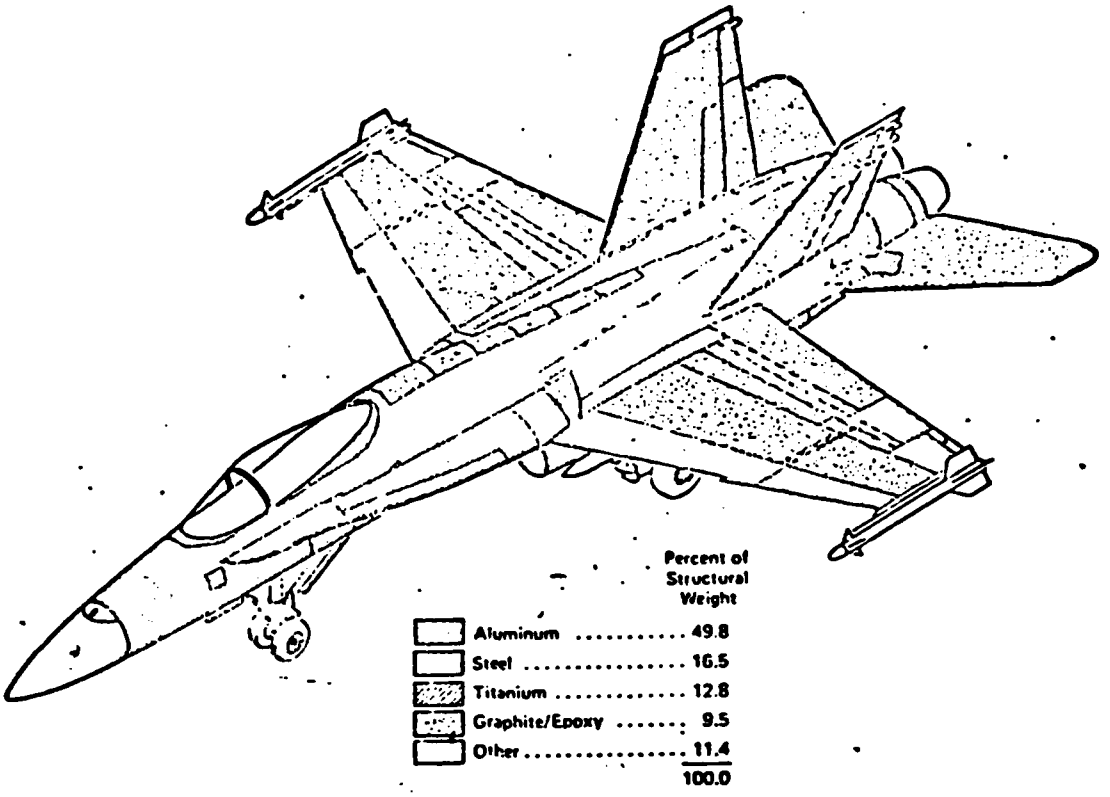

a. Upper Fuselage.

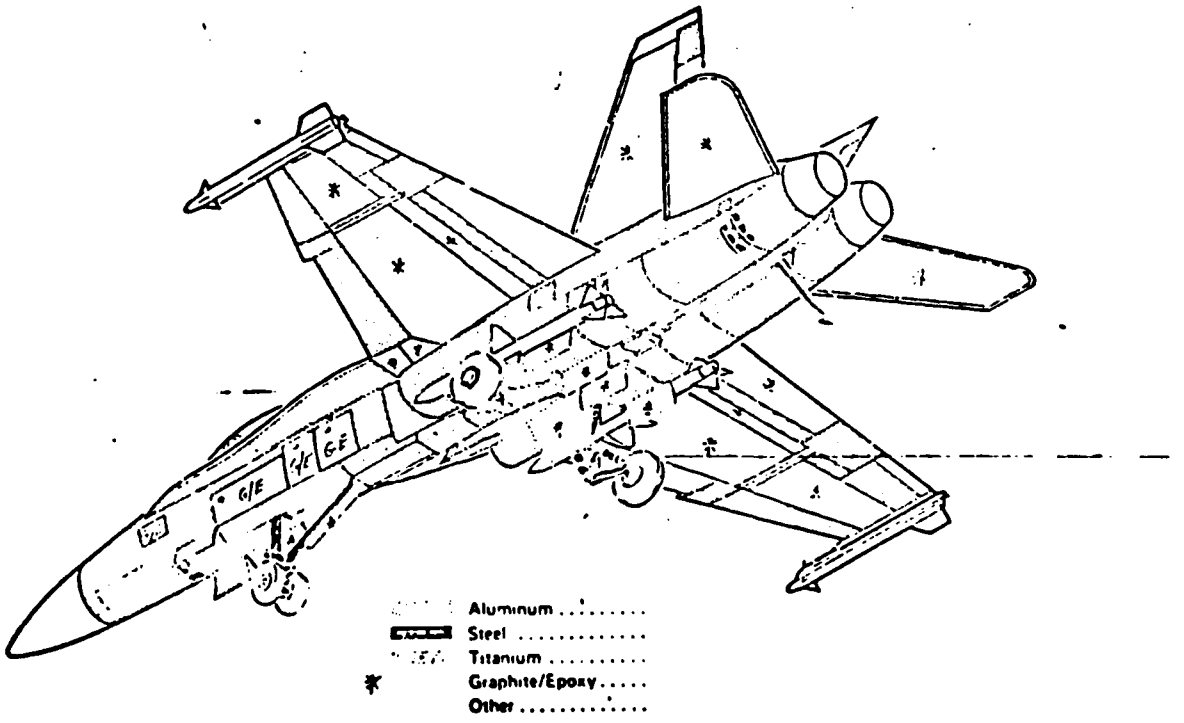

b. Lower Fuselage

Figure 1. F-18 Materials Distribution.

of these cables to these doors, lightning could induce spurious signals in these cables large enough to either damage or upset the attached electronics. These cables contain Balanced Twisted Shielded Pair (BTSP) wiring. The objective of this study is to therefore determine the lightning induced voltages and currents on the BTSP inner wires.

The approach in this study is to first examine the lightning threat and coupling paths to the F-18. Then the electromagnetic shielding and pertinent wiring practices are described. An overall computerized coupling model is then developed and implemented.

The analysis predicts that for a worst-case direct lightning stroke, the voltages on the BTSP wiring will be within the range of 16 to 175 volts. The differential mode is in the range of 0.5 to 5.3 volts.

CHAPTER 2

F-18 LIGHTNING COUPLING PATHS THROUGH THE AVIONICS BAY ACCESS DOORS

This section describes how transients from a lightning stroke attaching to the F-18 nose or tail can couple through the avionics bay access doors to the BTSP cables routed nearby.

The lightning current used in this report is the worst-case return stroke current of Figure 2, whose amplitude of 200,000 amperes exceeds more than 99% of all lightning strokes. The average return stroke current is on the order of 20,000 amperes. The spectral content in Figure 3 shows that lightning is mainly a low-frequency transient. The axial current is assumed to distribute uniformly around the fuselage, and the axial surface current density is therefore approximately

$$J_s \approx \frac{I}{2\pi r} = \frac{200\ Ka}{2\pi \times 0.72m} \approx 44\ Ka/m,$$

where the 0.72m radius of the fuselage at the avionics bay is used.

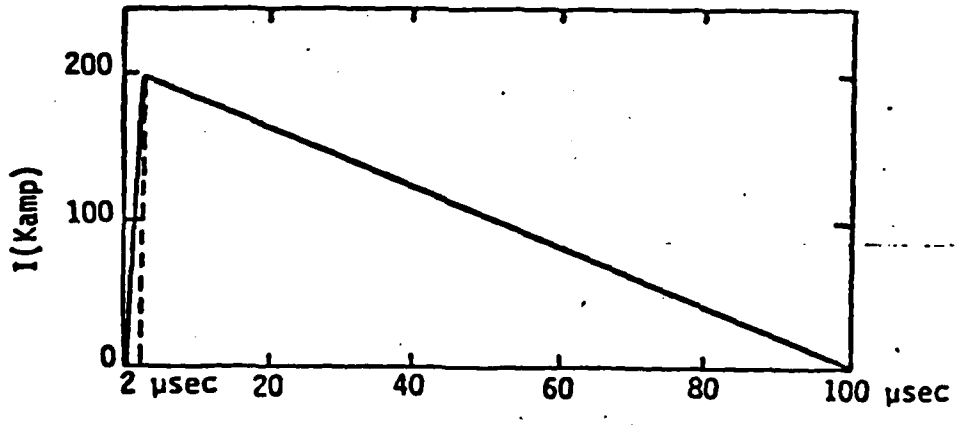

Figure 2. Lightning Return Stroke Current Used in the Direct Stroke Analysis.

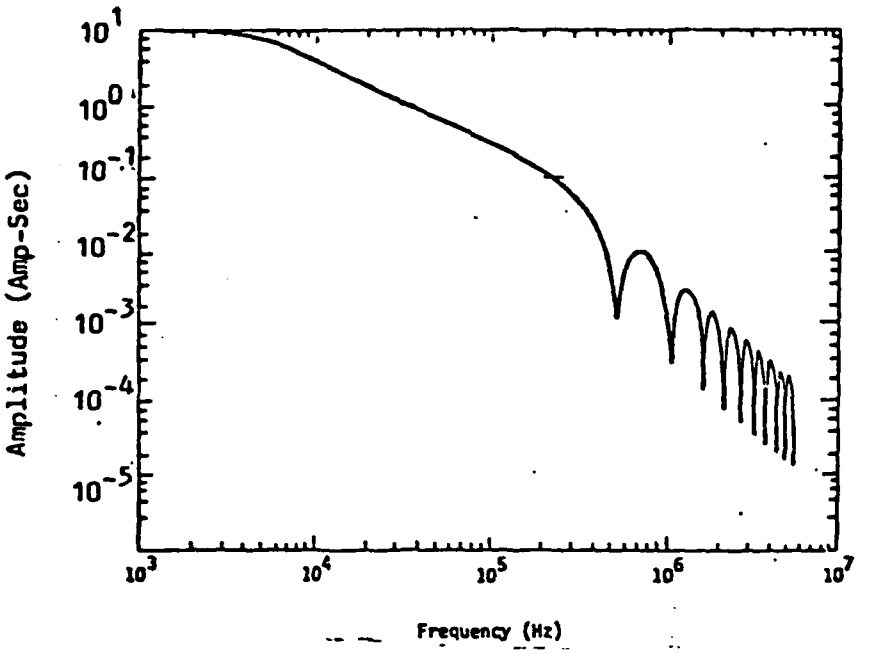

Figure 3. Spectral Amplitude of the Current Waveform of Figure 2.

This surface current density induces electromagnetic fields which can penetrate the fuselage through several different coupling mechanisms including:

1) diffusion of the fields through the skin,
2) voltage drops caused by surface currents flowing across electrically imperfect joints, such as seams or hinges,
3) direct penetration of the fields through cracks, holes, or apertures,
4) pickup on exterior cables that are routed through the skin to the fuselage interior, and
5) deliberate antennas.

Details of these coupling mechanisms are discussed in many places, including References 1 - 4. Because of the construction of the avionics bay doors, mechanism 3, above, is dominant.

The structural design of the avionics bay doors is indicated in Figure 4. The cables route in a bundle which is approximately two inches behind these doors. There are three doors on each side of the aircraft and they are located underneath and behind the cockpit, as shown in Figure 1b. The doors are made up of different cross-section layers, as summarized in Table 1, which also gives panel dimensions. We note that these doors are actually aluminum honeycomb sandwiched between layers of composite material. There is also an inner fiberglass layer.

Each access door in the avionics bay is attached to the fuselage by piano hinges, riveted along their entire length. The access doors are electrically bonded to the fuselage by bond straps connecting each end of the piano hinges to the fuselage. Additionally, the bottom edge of each access door is tightened down by the flush-mounted quick-release metallic fasteners.

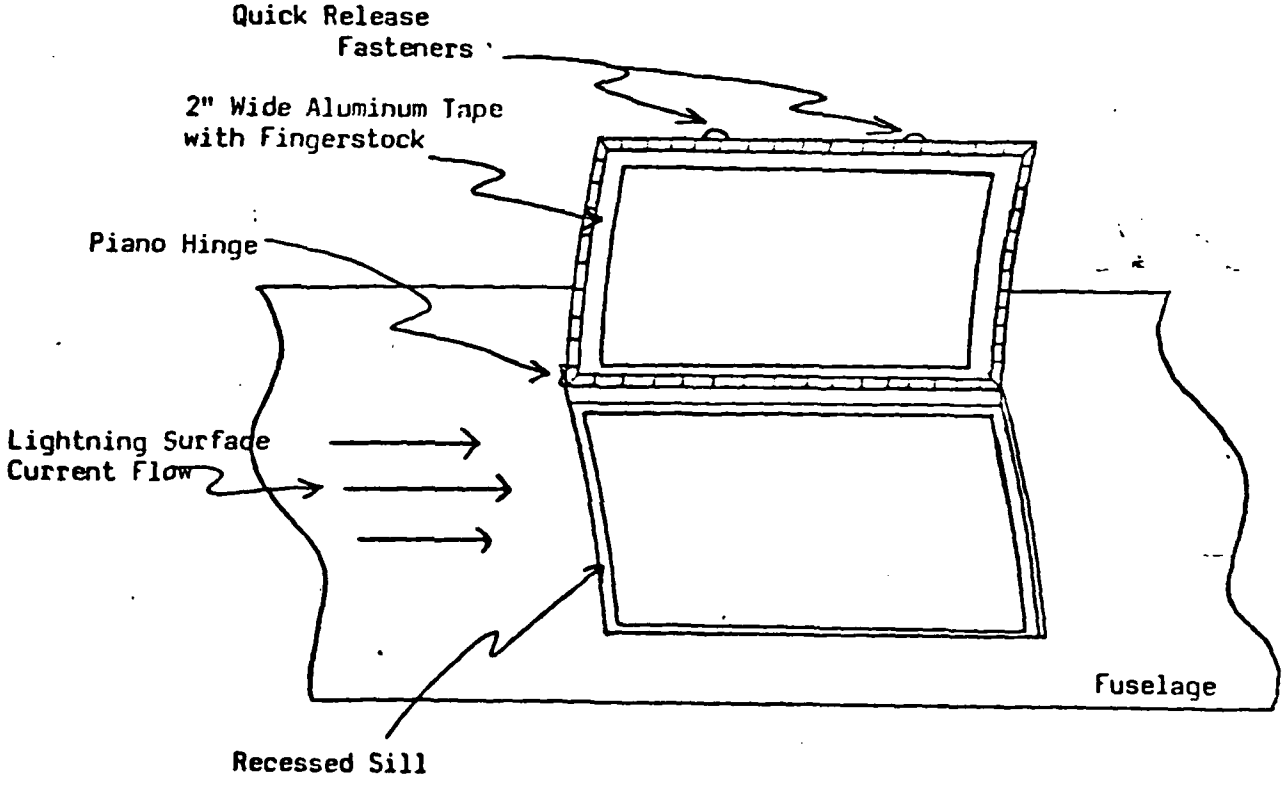

Figure 4. Illustration of Avionics Bay Doors Construction.

TABLE 1.

F-18 AVIONICS BAY ACCESS DOORS

Panel	Size
10 or 12	15" x 53"
13R or 13L	20" x 40"
14R or 14L	20" x 31"

Panel Cross-Section Construction

Outside Layer	5 ply Graphite Epoxy (5 mils/ply)
Middle Layer	Aluminum Honeycomb, 150 mils thick
Inside Layer	5 ply Graphite Epoxy (5 mils/ply)
	1 ply Fiberglass (5 mils/ply)

The layer of fiberglass is attached to the inside of the access doors to reduce the corrosion problem which occurs when graphite epoxy composites contact aluminum. A two-inch wide strip of aluminum tape with EMI fingerstock is attached around the periphery of the fiberglass layer to provide contact with the sill when the access doors are closed. However, except at perhaps the piano hinge and the fasteners, the aluminum tape is DC isolated (capacitively coupled) from the access door by the fiberglass layer.

For a stroke to the nose or tail and exiting the tail or nose, the surface current density in the vicinity of these doors is principally axial and was previously calculated to be 44 Ka/m. If the door did not affect the surface current distribution, it would flow in a direction parallel to the edges of the door which are DC connected, and normal to the edges which are not DC connected. Thus the edges which are normal to the flow are cracks which can be modelled as a capacitively loaded slot antenna (Reference 1). The capacitance loading between the aluminum tape on the access doors and the doorpanel on the fuselage, can be estimated by well-known standard formulas for parallel plate capacitors, and one obtains

10.6 nf/m for a relative dielectric constant of 3 for the 5-mil layer of fiberglass. Corrosion and vibration of the access doors does not affect this capacitance.

It is noted that these slots exist independently of whether or not the door edges parallel to the current flow are DC connected (which they are). In addition, because there are three doors, there are six slots.

For the purposes of this investigation therefore, coupling of the lightning current to the cables is limited to that caused by the aforementioned slots which are normal to the axial lightning current flow. It is noted that diffusion through the door is neglected. This is because the aluminum honeycomb will tend to short out the electric field and reduce the diffusion fields to a small value. The actual modelling of the slot coupling is reserved for Chapter 4. Before this model is presented, the cabling and shielding practices in the F-18 are discussed in Chapter 3, along with features pertinent to the present analysis.

CHAPTER 3

F-18 SHIELDING AND CABLING PRACTICES

The general design philosphy for EMI mitigation on internal cables and boxes is to use filters or filter pin connectors at the box inputs to reduce the high frequency signals, shielded cables to reduce the middle frequencies, and balanced loads for the low frequencies. Balanced Twisted Shielded Pair (BTSP) cables are frequently used to implement this shielding philosophy, particularly for connections to the flight control computer.

The physical layout of the cabling determines coupling to the cables. The wires in the F-18 are grouped together into wiring harnesses (or bundles) about two inches in diameter and supported about two inches away from the fuselage skin. A typical harness consists of many types of cables, both shielded and unshielded, single and multiconductor. The ends of the cable shields are brought out in pigtails four to eight inches long and bonded to the electronic box shield (which is bonded to the airframe structure) via a connector pin. The connectors use plastic backshells, which are lightweight but offer no shielding. Therefore, connector shielding degradation caused by vibration and corrosion are not pertinent and thus not considered here. Also, because lightning is of mainly low frequency content, filter pin connectors offer little attenuation, and in fact can degrade differential mode attenuation at the low frequencies.

Cable shielding will now be defined and discussed, first in general terms, and then specifics relating to the BTSP will be given.

A shielded cable which routes over a structure or ground plane allows spurious signals to appear on the inner conductors by two mechanisms: the shield transfer impedance $Z_t(\omega)$ and the shield transfer admittance $Y_t(\omega)$. These are defined in terms of the shield current $I_s(\omega)$, shield voltage with respect to structure $V_s(\omega)$, the induced electric field $E_i(\omega)$ on the inside of the shield, and the induced internal current sources per unit length

$I_i(\omega)$ according to

$$E_i(\omega) = Z_t(\omega)\, I_s(\omega)$$

$$I_i(\omega) = Y_t(\omega)\, V_s(\omega) \ .$$

The wires inside the shield can be adequately modelled by standard TEM transmission line telegrapher's equations which are, for a single wire,

$$\frac{dV}{dx} = -ZI + Y_t V_s \ , \text{ and}$$

$$\frac{dI}{dx} = -YV + Z_t I_s \ ,$$

where V is the voltage on the wire at a spatial coordinate x, I the current on the wire, V_s and I_s the distributed voltage and current sources defined above, and Z and Y the per unit length series impedance and shunt admittance of the wire. Z is the transmission line inductance and a series line resistance, and Y is the line capacitance. These equations can be modelled as a distributed circuit, with an elemental section of length dx shown in Figure 5.

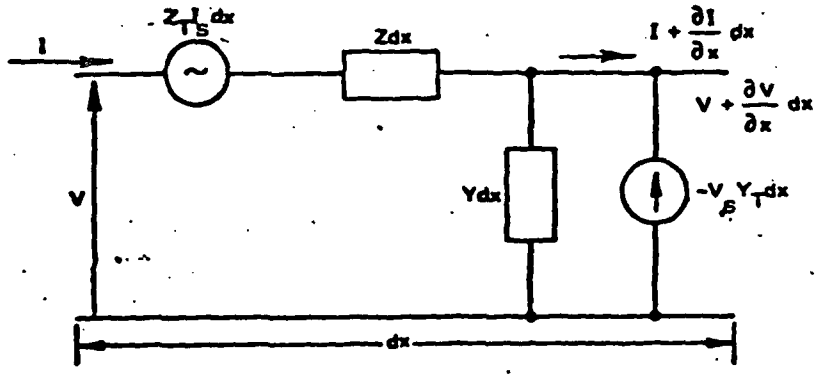

Figure 5. Inner Conductor Equivalent Circuit When Both the Transfer Impedance and the Transfer Admittance Are Included.

For a solid shield, the transfer admittance is zero, and the transfer impedance is a diffusion mechanism only, and is a monotonically

decreasing function with frequency. A braided shield however, has many small apertures at the junctions where the individual wires of the shield do not overlap each other. These apertures allow penetration by higher frequencies. The transfer impedance now includes a transfer inductance caused by the aperture magnetic dipole moment and the transfer admittance is caused by the aperture electric dipole moment. This causes a decrease in shielding effectiveness at high frequencies, as shown in Figure 6, which compares the transfer impedance of solid and braided shields.

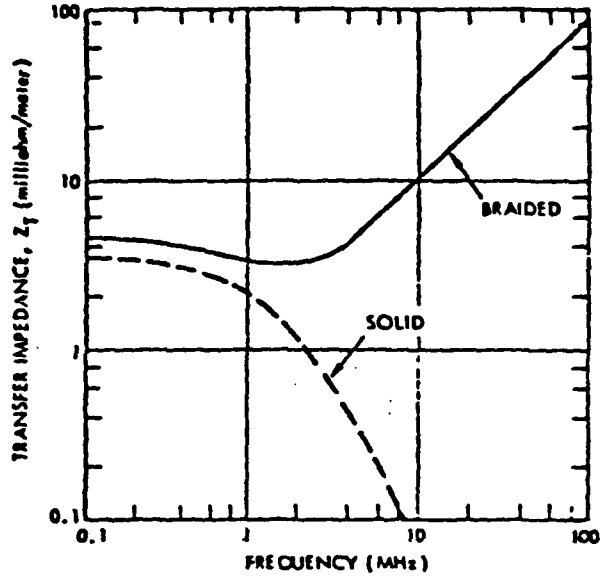

Figure 6. Transfer Impedance of Braided and Solid Outer Conductor Coaxial Cable.

The frequency domain transfer impedance for a braided shield can be represented as

$$Z_t = R_t + j\omega L_t$$

with R_t the transfer resistance of the shield, and L_t the transfer inductance.

The characteristics of a braided shield are defined in terms of the radius r of the shield, the number of carriers C (belts or wires), the

picks P (number of carrier crossings per unit length), and ends N (number of wires in each carrier), and the individual wire diameter d [5].

A typical braided pattern is shown in Figure 7. The pitch angle α is given by

$$\alpha = \tan^{-1} \frac{4\pi aP}{C}$$

and the coverage of one carrier is

$$F = \frac{PNd}{\sin\alpha} .$$

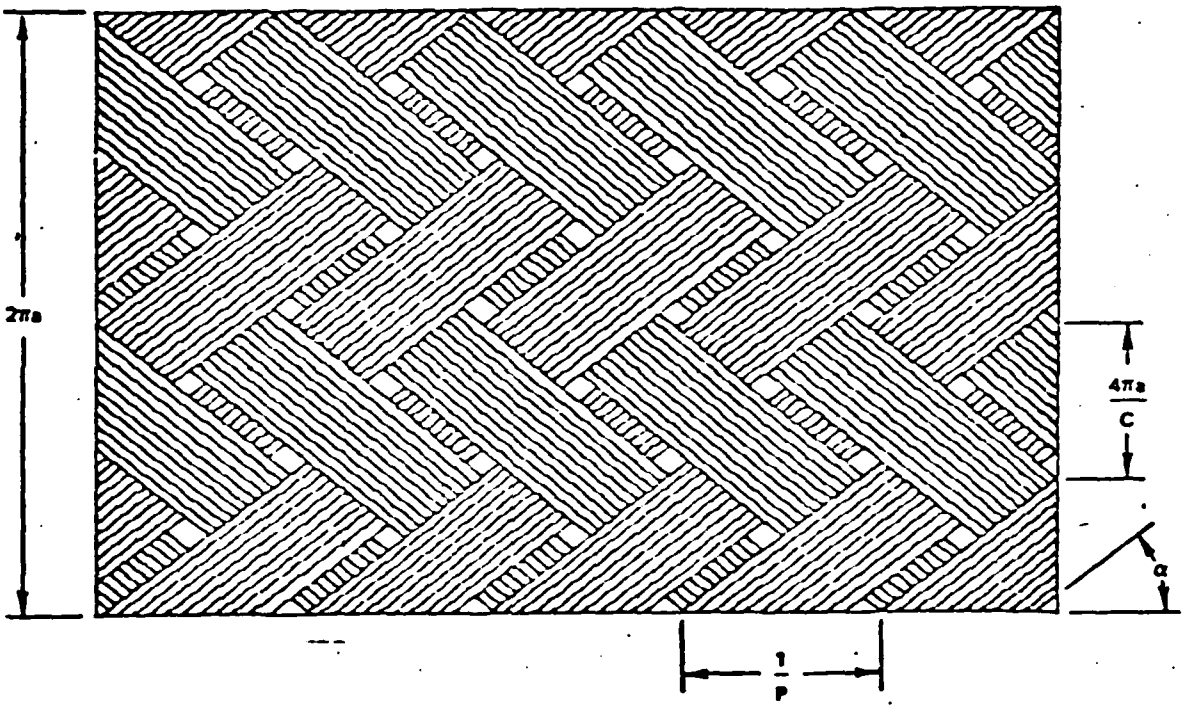

Figure 7. Braided Pattern Developed on a Plane.

A useful item is the optical coverage of the shield, which is equal to

$$K = 2F - F^2 .$$

Typical braided shields have optical coverages of from 85 to 95 percent and

an α of 30° to 45°. Figures 8 and 9 show how the different parameters affect the shielding effectiveness of braided shields, which is defined by

$$\text{Cable Shielding Effectiveness} = 20\log_{10}\frac{I_s}{I_{ic}}$$

with I_s the shield current, and I_{ic} the inner conductor current.

The transfer resistance of the shield is

$$R = \frac{1}{\pi^2 r d \sigma f \cos^2\alpha}\,\frac{\gamma d}{\sinh\gamma d}$$

with

$$\gamma = \sqrt{j\omega\mu\sigma}\ ,$$

and the transfer inductance is given by

$$L = \frac{\pi\mu}{6C}(1-K)^{3/2}\,\frac{e^2}{E(e^2)-\tan^2\alpha K(e^2)}$$

with

$$e^2 = 1-\tan^2\alpha$$

and $K(e^2)$ and $E(e^2)$ the complete elliptic integral of the first and second kind.

The transfer admittance is given by

$$Y_t = -j\omega C_1 C_2\,\frac{\pi}{6\epsilon C}(1-K)^{3/2}\,\frac{1}{E(e^2)}$$

with C_1 and C_2 the capacitances between the shield and ground, and the shield and the inner conductor respectively. However, the transfer admittance is so small, that it can usually be ignored [6].

The cross-sections of two F-18 BTSP cables are shown in Figure 10, and are arbitrarily labeled BTSP #1 and BTSP #2 for easy referencing. Table 2 shows the parameters calculated for these cables. The transfer admittance, Y_t, is neglibible and is not used further. Therefore, only

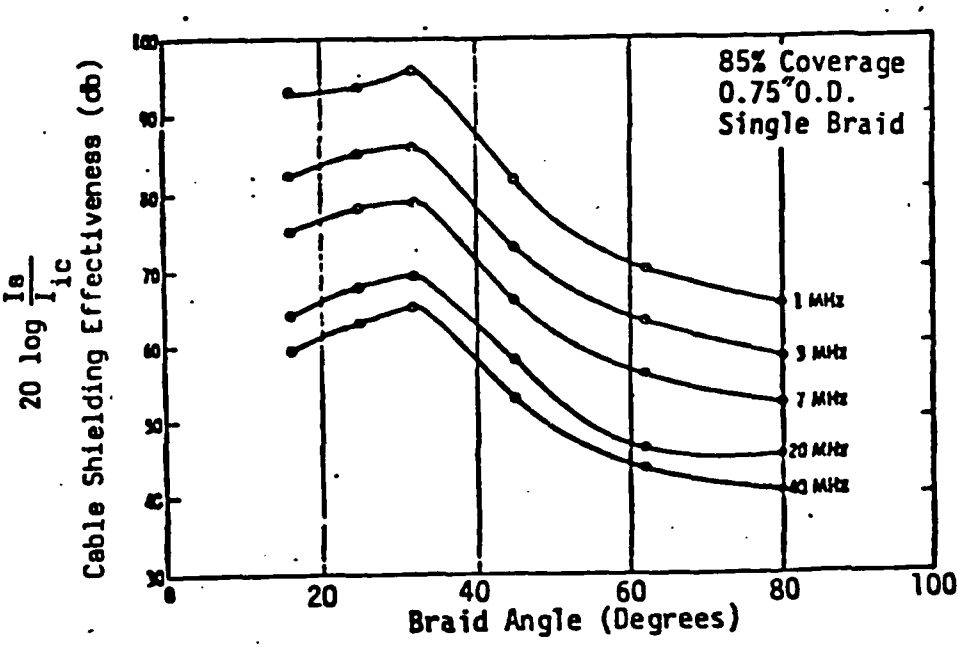

Figure 8. Braid Angle [2].

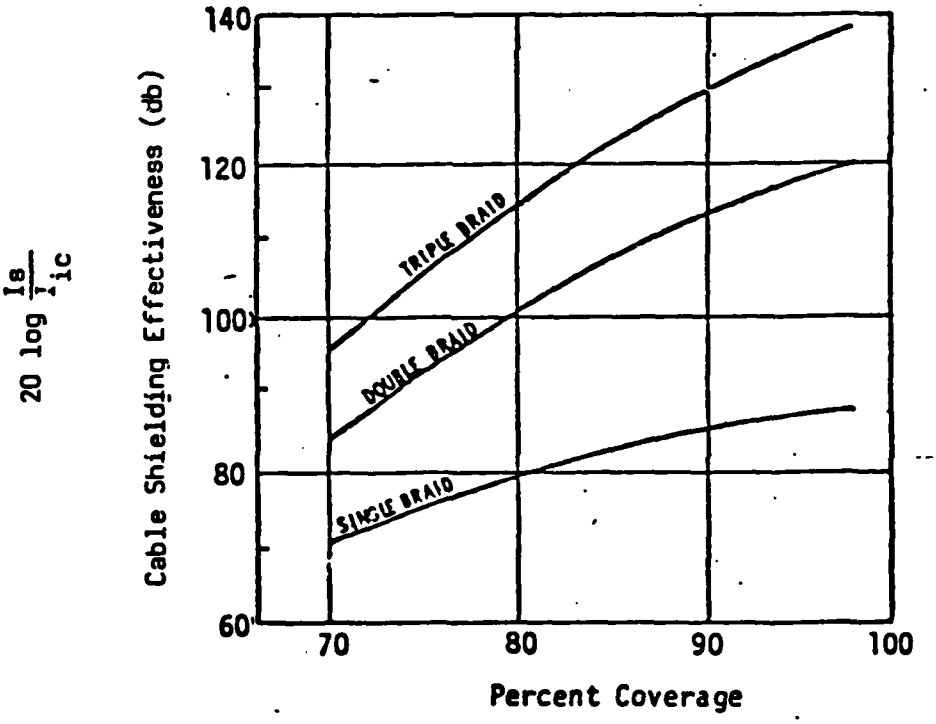

Figure 9. S.E. Change with Percent Optical Coverage [2].

the shield current drives the inner conductors, and knowledge of the shield current is sufficient to determine the BTSP responses.

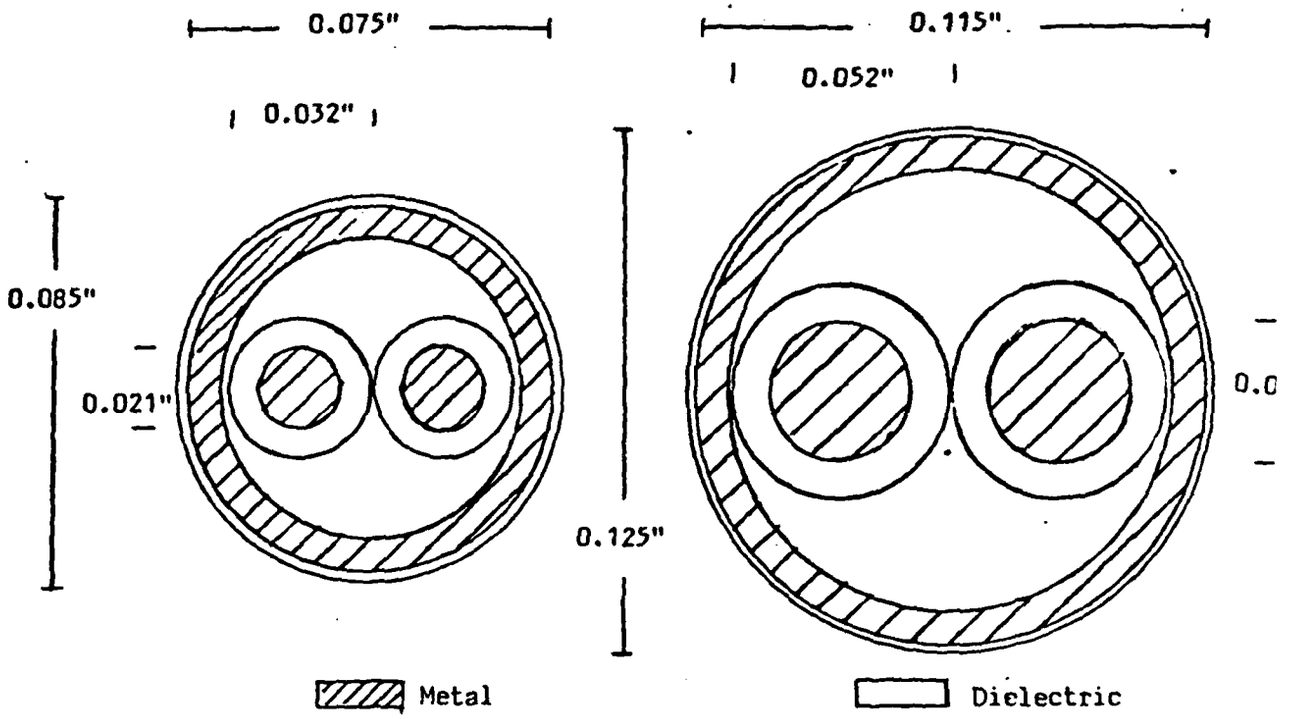

Figure 10. Two BTSP Cables.

TABLE 2.

PARAMETERS OF THE TWO BTSP CABLES

		BTSP #1	BTSP #2
Z_{C_s}	=	107 Ω	255 Ω
L_s	=	0.36 μH/m	0.85 μH/m
C_s	=	31 pf/m	13 pf/m
R_s	=	54 mΩ/m	36 mΩ/m
$C_{ic_{11}}$	=	60 pf/m	212 pf/m
$C_{ic_{22}}$	=	60 pf/m	212 pf/m
$C_{ic_{12}}$	=	16 pf/m	3 pf/m
$L_{ic_{11}}$	=	199 nH/m	52 nH/m
$L_{ic_{22}}$	=	199 nH/m	52 nH/m
$L_{ic_{12}}$	=	54 nH/m	0.78 nH/m
R_{ic}	=	136 mΩ/m	28 mΩ/m
K	=	83 %	85 %
$L_{pigtails}$	=	0.23 μH	0.22 μH
Z_t	=	54 mΩ/m+jω3nH/m	36 mΩ/m+jω3nH/m
Y_t	=	+jω0.43 pf/m	+jω0.50 pf/m

Note: The subscript s refers to the shield parameters, and the subscript ic refers to the two inner conductors.

CHAPTER 4

THE OVERALL COUPLING MODEL AND NUMERICAL RESULTS

In Chapter 2, we showed that the coupling path to cables behind the avionics bay doors can be modelled as a capacitively loaded slot antenna. In Chapter 3, we discussed the cabling practices and defined the shielding parameters for the BTSP cables. In Chapter 4, we will now present the overall combined coupling model and present the numerical results.

The overall coupling problem is shown pictorially in Figure 11. The figure shows two electronics boxes, each bonded to the airframe or skin, with a wiring harness or bulk cable connecting the two boxes. The bulk cable contains 10 or 20 separate cables, including at least one single BTSP cable. The desired information is the voltage induced on the BTSP internal wires.

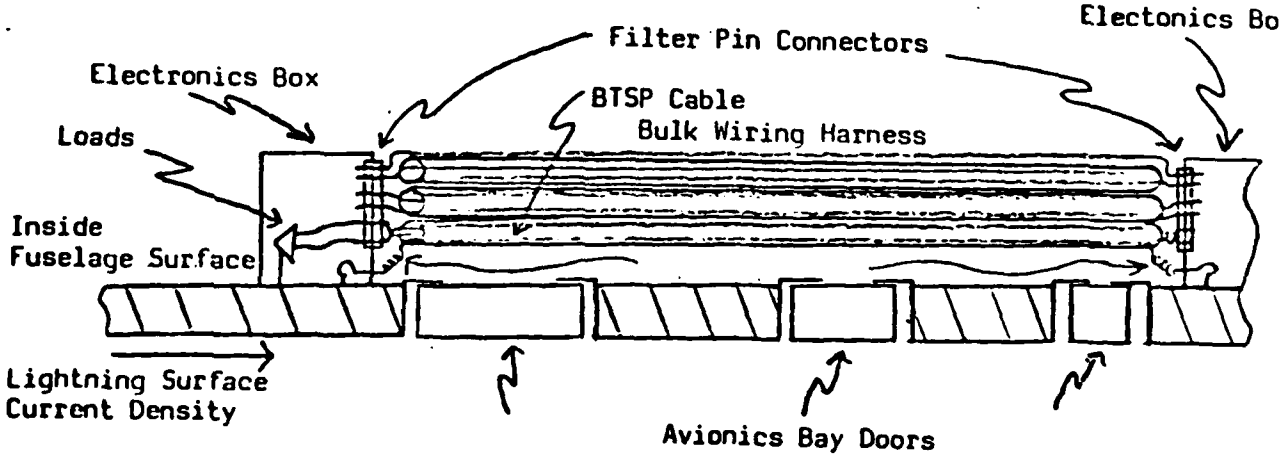

Figure 11. Pictorial Representation of Overall Coupling Problem.

We also note that the BTSP internal wires can be connected to balanced loads on each end. Another configuration is possible, namely, that the load may be unbalanced at one end (one wire connected to structure) and balanced at the other.

Indicated on the skin are the three avionics bay doors which have a total of six slots which are normal to the surface current flow.

The analysis procedure is summarized by first determining a circuit model for the coupling of the lightning induced skin current to the bulk cable. The result is the sum total bulk current flowing in the bulk cable wiring harness. The next step is to partition this current and determine a reasonable estimate of the current on the single BTSP shield. Then the BTSP shield current is used to determine the electric fields inside of it by means of the shield transfer impedance. These fields are sources which drive the internal wires which are solved by a multiconductor TEM transmission line code [7, Appendix A]. We note that coupling from the pigtails and exposed terminations is negligible at these frequencies compared to the other effects.

The slot model follows that of Reference 1, and is summarized in Figure 12, which shows the duality between a slot in a perfect conductor and a strip dipole in free space, both of which are small in terms of wavelength.

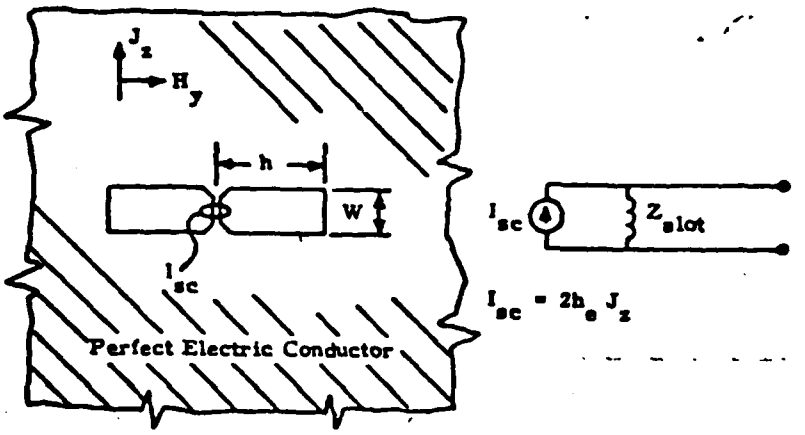

a. Slot Antenna.

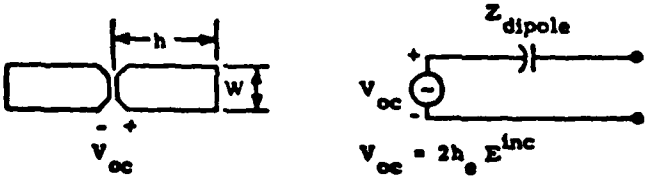

b. Complementary Strip Dipole.

Figure 12. A Slot Antenna and Its Complementary Strip Dipole.

The avionics bay panels have h=10" and w=5 mils, with

$$\Omega = 2\ln\frac{8h}{w} = 2\ln\frac{8\times10"}{0.005"} = 19.4,$$

where Ω is the fatness factor for strip dipoles. The effective height is given by

$$h_{e(\text{dipole})} = h_{e(\text{slot})} \approx \frac{h}{2} = 5"$$

which is valid for large fatness factors. The short circuit current is therefore

$$I_{sc} = 2h_e J_{Axial} \approx 11 \text{ Ka.}$$

The impedance of the strip dipole is capacitive, which is given by

$$C = \frac{h \text{ (meters)}}{1.8\times10^{10}(\Omega-3.39)} \approx 0.88\text{pf.}$$

The impedance of the slot antenna is related to the strip dipole impedance by

$$Z_{slot} = \frac{(60\pi\text{ohms})^2}{Z_{dipole}} = \frac{(60\pi\text{ohms})^2}{1/j\omega C} \approx j\omega 31\times10^{-9}.$$

Thus the slot inductance is 31nH.

Loading the slot antenna is a capacitance between the aluminum tape and the door panel, which, for a 20" slot is approximately 5.4 nf.

Also, the series impedance of the nearby bulk cable loads the circuit. Since the harness is about two inches in diameter, and about two inches above the fuselage, its characteristic impedance as given for a wire over a ground plane is approximately 83Ω, which has an inductance per unit length of .277μH/m. Assuming the cable is ten meters long gives a total series inductance of 2.8μH. The series resistance of the bulk cable is negligible.

The load of the bulk cable on the slot is strictly speaking the input impedance of a transmission line short circuited on the ends (the bulk cable has enough shielded cables connected to structure on each end

to provide low impedance terminations). However, because the cable lengths are very small fractions of a wavelength long, the impedance consists only of the line inductance, 2.8μH.

The equivalent circuit of the loaded slot antenna is now complete, and is shown in Figure 13. The slot capacitance is unimportant for lightning frequencies because its impedance is much higher than the inductors'. We also note that the six slots are simply added together. The current flowing on the bulk cable is obtained by a current divider based on the inductances, from which one obtains 722 amperes.

The next problem is to determine how much current can actually be flowing on a single BTSP shield. If there are N conductors in the bundle, the average current flowing on any one cable is 1/N times the total bulk current. We assume N is approximately 20 for the bundle, and obtain 36 amperes on the BTSP shield. The real answer is probably more than this, however, because cables on the outside of the bundle would carry more than those on the inside, and cables nearest the ground plane would carry more than those elsewhere in the bundle.

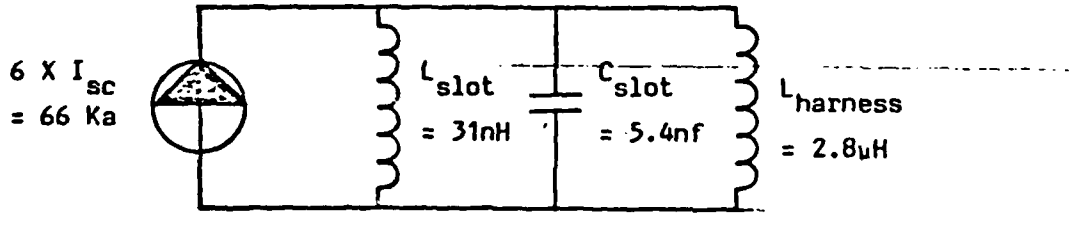

Figure 13. Equivalent Circuit of the Avionics Bay Coupling Mechanism.

In order to obtain an upper bound estimate of the BTSP shield current, the geometry of Figure 14 was adopted. The BTSP cable is placed directly under the bulk cable and one insulation thickness away. At lightning frequencies, the current divides between the two cables according to

$$I_{BTSP} = I_{Bulk} \frac{j\omega(L_B+M)}{R_W+j\omega(L_B+L_W+2M)}$$

with

R_W - the resistance of the individual wire,

L_B and L_W - the self inductances of the bulk cable and the single wire, and

M - the mutual inductance between the bulk cable and the individual wire.

Again, the resistance of the bulk cable is assumed to be negligible.

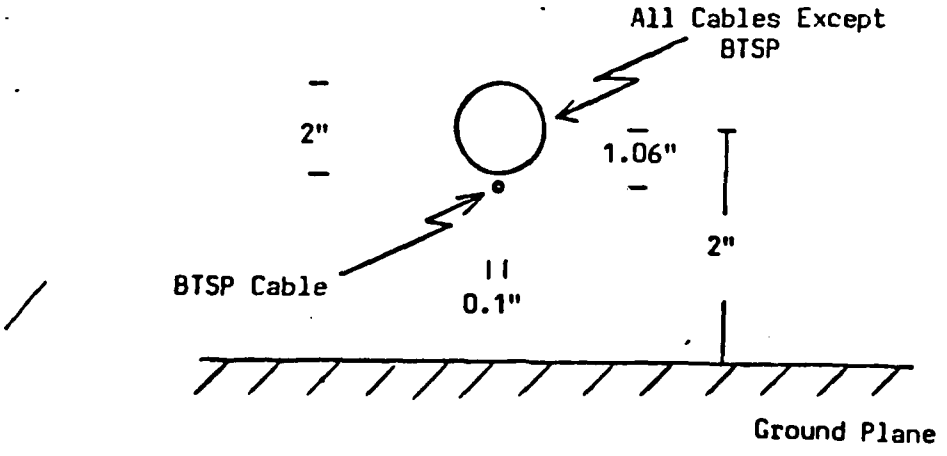

Figure 14. Wire Configuration for Worst-Case Current Division.

TABLE 3.

SUMMARY OF VALUES FOR CURRENT DIVISION

	BTSP #1	BTSP #2
R_W	0.54 Ω	0.36 Ω
L_B	0.26 μH	0.26 μH
L_W	0.47 μH	0.54 μH
M	0.24 μH	0.25 μH

Table 3 summarizes the values used to obtain this current sharing. The inductance values are obtained from EMA's CAPCODE [8] computer code.

The resulting current division is frequency dependent. Peak currents of 277 A and 270 A were calculated for BTSP numbers 1 and 2, respectively.

Because the transfer inductance of the shield is on the order of 3nH/m, it does not play a role in shielding effectiveness until about 1mHz. The internal voltage on the BTSP cables can then be estimated by taking the product of the transfer resistance, the cable length, and the shield current. A better calculation can be done by using the code BTSP which is discussed in Appendix A.

The results for peak induced BTSP shield currents and induced voltages on the center wires are summarized in Table 4. V_{CM} is the common mode voltage, and V_{DM_1} is the differential mode voltage across a balanced load without filter pin connectors. V_{DM_2} is the voltage across a balanced load with filter pin connectors. The value for V_{DM_1} is obtained from the V_{CM} based on experimental results taken by EMA personnel on similar BTSP cables measured by injecting lightning waveform current pulses on the cable shields [9]. These results showed that V_{DM_1} was about 3% of V_{CM}. V_{DM_2} is determined based on data taken by F-18 contractor personnel [10]

of wire voltage as a function of frequency for three different wire configurations for an incident field on the F-18. At 300 kHz, the lower frequency limit of the data, the presence of filter pin connectors increases the differential mode voltage by a factor of 25. At lower frequencies it is probably not this much, so this factor is a worst-case. Thus we have taken $V_{DM_2} = 25\ V_{DM_1}$. V_{DM_2} is thus the expected result applicable to the F-18 balanced loads. We also note that some loads are only balanced at one end, and in this case, V_{DM_1} is equal to V_{CM}. On an unshielded wire, the maximum voltage possible is 1023 volts, which is the open circuit voltage of all six slots added together.

TABLE 4.

SUMMARY OF COUPLING RESULTS (VOLTS)

	Average Case				Worst Case			
	I_{BTSP} (Amps)	V_{CM} (Volts)	V_{DM_1} (Volts)	V_{DM_2} (Volts)	I_{BTSP} (Amps)	V_{CM} (Volts)	V_{DM_1} (Volts)	V_{DM_2} (Volts)
BTSP #1	36	23	0.7	18	277	175	5.3	133
BTSP #2	36	16	0.5	13	270	123	3.7	93

The computed voltage waveforms V_{CM} for the worst-case division are given in Figure 15.

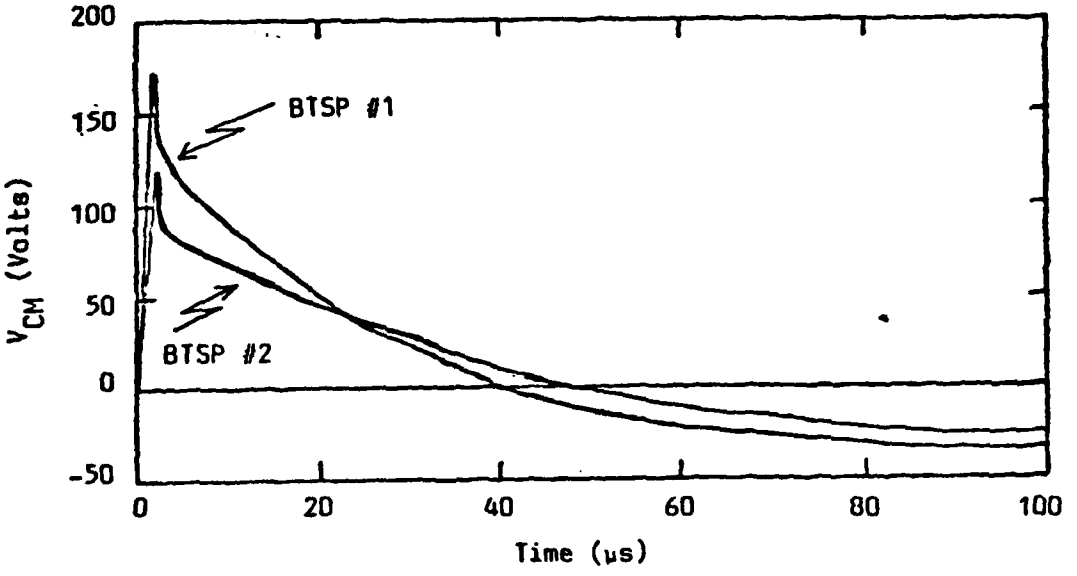

Figure 15. Induced BTSP Common Mode Voltages for Worst-Case Division.

CHAPTER 5

SUMMARY AND CONCLUSIONS

The analytical results show that BTSP inner wire common and differential mode voltages for a worst case lightning stroke are in the nominal range of 16-175 volts and 0.5-5.3 volts, respectively. It is observed that this worst case stroke occurs much less than 1% of all lightning strokes (Figure 16), and an average value would be approximately 10% of the above values.

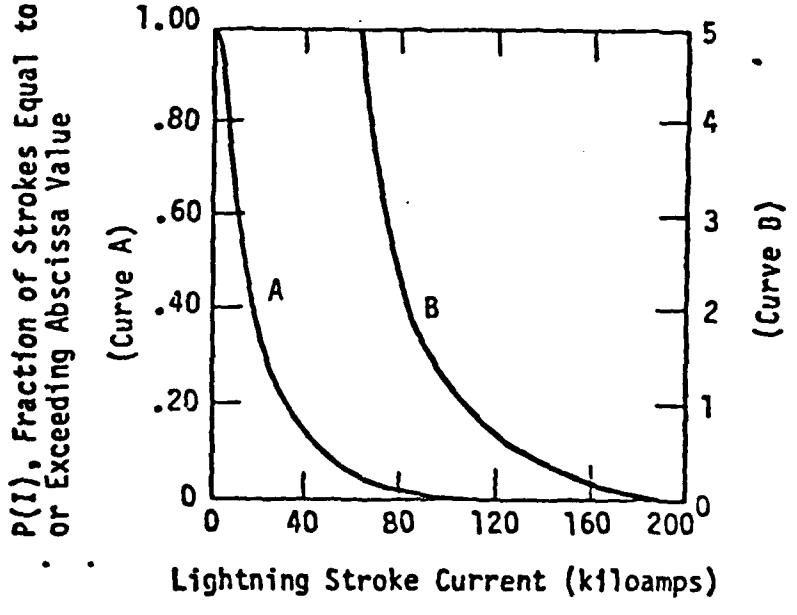

Figure 16. Lightning Stroke Current Probability Curve.

Several assumptions were made in this analysis:

1. The six slots were assumed to be mutually decoupled.
2. The slot excitation of the bulk cable was assumed to not depend upon the distance between the cable and the slots.
3. Coupling estimates included the avionics bay doors only; no other coupling paths were included, and there likely are some others.

Table 5 summarizes our results for a BTSP cable excited by the F-18 avionics bay doors. We have also included results for a near-miss worst-case lightning stroke (50 meters away), which results in 2% of the surface current of a direct strike. The voltages are similarily scaled.

We point out that the results are based on a linear analysis. That is to say, a full-threat level lightning stroke may cause arcing to occur at significant points and change the coupling response. The response may be either larger or smaller than that predicted by the linear analysis. Nonlinear effects are quite difficult to predict, and can be accurately determined only by a threat-level test.

TABLE 5.

SUMMARY OF COUPLING RESULTS FOR 200 KA LIGHTNING STRIKE

Units are volts and are time domain peak values

	Direct Stroke	Near Miss
V_{DM} without filter pin connectors	0.5-5.3	0.010-0.106
V_{DM} with filter pin connectors	13-133	0.26-2.7

REFERENCES

1. D. E. Merewether, et. al, Electromagnetic Pulse Handbook for Missles and Aircraft in Flight, SC-M-710346, Sandia Laboratories, Sept. 1972.

2. R. A. Perala and T. F. Ezell, Engineering Design Guidelines for EMP Hardening of Naval Missiles and Airplanes, AMRC-R-17, Mission Research Corporation, Dec. 1973.

3. K. M. Lee, R. A. Perala, and R. B. Cook, Induced Effects of Lightning on the Advanced Design Composite Aircraft, AMRC-R-137, Mission Research Corporation, July 1978.

4. D. Strawe and L. Piszker, Interaction of Advanced Composites with Electromagnetic Pulse (EMP) Environment, AFML-TR-75-141, Boeing Aerospace Company, Sept. 1975.

5. E. F. Vance, Shielding Effectiveness of Braided Wire Shields, Interaction Note 172, April 1974.

6. D. E. Merewether and T. F. Ezell, The Effect of Mutual Inductance and Mutual Capacitance on the Transient Response of Braided-Shield Coaxial Cables, IEEE Trans. EMC, Feb. 1976.

7. R. A. Perala, Excitation Functions for Multiconductor Transmission Lines Illumined by Nonuniform Electromagnetic Fields, AMRC-R-24 Mission Research Corporation, June 1974.

8. L. Licking, Capacitance Analysis for Arbitrary Cylindrical Geometries; Application to Electromagnetic Coupling into Subsystems Through Cables, SC-RR-72-0299, Sandia Laboratories, May 1972.

9. R. A. Perala, R. B. Cook, and J. D. Robb, Support of Lightning Analysis and Testing on the Solid Rocket Booster (SRB) Vehicle, AMRC-R-122, Mission Research Corporation, March 1978.

10. G. Weinstock, Viewgraphs presented at NAVAIR, on 5 March, 1979, McDonnell Aircraft Company, St. Louis, Missouri.

APPENDIX A

THE FORMULATION OF THE BTSP COMPUTER PROGRAM

The frequency domain responses of a two-wire multiconductor transmission line are governed by the telegrapher's equations given by

$$\frac{d}{dx}[V] = -[Z][I]+[\sum_m A_m e^{i\alpha_m x}] \text{ and}$$

$$\frac{d}{dx}[I] = -[Y][V]+[\sum_m B_m e^{i\beta_m x}]$$

with the following definitions

$[V]$ - a 2x1 column matrix of the voltages from each wire to ground.

$[I]$ - a 2x1 column matrix of the currents on each wire.

$[Z]$ - a 2x2 matrix of the series impedances of each wire. with $Z_{ij} = R_{ij}-i\omega L_{ij}$.

$[Y]$ - a 2x2 matrix of the shunt admittances of each wire with $Y_{ij} = -G_{ij}+i\omega C_{ij}$ and $Y_{ii} = \sum_j G_{ij}-i\omega C_{ij}$.

$[\sum_m A_m e^{i\alpha_m x}]$ - a 2x1 column matrix representing the superposition of m distributed voltage sources.

$[\sum_m B_m e^{i\beta_m x}]$ - a 2x1 column matrix representing the superposition of m distributed current sources.

R_{ij}, L_{ij}, G_{ij}, C_{ij} - the series resistance and inductance, and shunt conductance and admittance between wires i and j.

α_m, β_m - the propagation constants of the distributed voltage and current sources.

One solution of these equations is

$$[V] = [R]\, e^{i\gamma x} +[S]\, e^{-i\gamma x} +[\sum_m M_m e^{i\alpha_m x}]+[\sum_m N_m e^{i\beta_m x}] \text{ and}$$

$$[I] = [T]\, e^{i\gamma x} +[V]\, e^{-i\gamma x} +[\sum_m P_m e^{i\alpha_m x}]+[\sum_m Q_m e^{i\beta_m x}]$$

with

$[R]$ - a 2x1 row matrix representing the amplitudes of the forward traveling voltage wave.

$[S]$ - a 2x1 row matrix representing the amplitudes of the backward traveling voltage wave.

$[\sum_m M_m e^{i\alpha_m x}]$ - a 2x1 column matrix representing the superposition of the voltage responses from the voltage sources.

$[\sum_m N_m e^{i\beta_m x}]$ - a 2x1 column matrix representing the superposition of the voltage responses from the current sources.

$[T]$ - a 2x1 row matrix representing the amplitudes of the forward traveling current wave.

$[V]$ - a 2x1 row matrix representing the amplitudes of the backward traveling current wave.

$[\sum_m P_m e^{i\alpha_m x}]$ - a 2x1 column matrix representing the superposition of the current responses from the voltage sources.

$[\sum_m Q_m e^{i\beta_m x}]$ - a 2x1 column matrix representing the superposition of the current responses from the current sources.

$e^{i\gamma x}$ - a scalar representing a forward traveling wave.

$e^{-i\gamma x}$ - a scalar representing a backward traveling wave.

γ - the propagation constant of the wires (both wires are assumed to have the same propagation constant).

The homogeneous solution gives the following relationships

$$[T] = \frac{-1}{i\gamma}[Y][R] \quad \text{and} \quad [U] = \frac{1}{i\gamma}[Y][S] \ .$$

Furthermore, if we define

$$[G] = [Z][Y]$$

then $\gamma^2 = -Z_{11}Y_{11}$, for a single-wire becomes,

$$\gamma^2 = \frac{-(G_{11}+G_{22}) \pm \sqrt{(G_{11}-G_{22})^2 + 4\,G_{12}G_{21}}}{2} \quad \text{for two wires.}$$

The particular solution gives the following for the mth source

$$\begin{bmatrix}[M_m]\\ [P_m]\end{bmatrix} = \begin{bmatrix}[i\alpha_m] & [Z]\\ [Y] & [i\alpha_m]\end{bmatrix}^{-1}\begin{bmatrix}[A_m]\\ [0]\end{bmatrix} \quad \text{and}$$

$$\begin{bmatrix}[N_m]\\ [Q_m]\end{bmatrix} = \begin{bmatrix}[i\beta_m] & [Z]\\ [Y] & [i\beta_m]\end{bmatrix}^{-1}\begin{bmatrix}[0]\\ [B_m]\end{bmatrix}$$

with the following definitions for a two-wire line,

$$[M_m] = \begin{bmatrix} M_{1m} \\ M_{2m} \end{bmatrix}, \quad [N_m] = \begin{bmatrix} N_{1m} \\ N_{2m} \end{bmatrix}, \quad [P_m] = \begin{bmatrix} P_{1m} \\ P_{2m} \end{bmatrix}, \quad [Q_m] = \begin{bmatrix} Q_{1m} \\ Q_{2m} \end{bmatrix}, \text{ and}$$

$$[i\alpha_m] = \begin{bmatrix} i\alpha_{1m} & 0 \\ 0 & i\alpha_{2m} \end{bmatrix}, \quad [i\beta_m] = \begin{bmatrix} i\beta_{1m} & 0 \\ 0 & i\beta_{2m} \end{bmatrix}, \quad [A_m] = \begin{bmatrix} A_{1m} \\ A_{2m} \end{bmatrix}, \text{ and } [B_m] = \begin{bmatrix} B_{1m} \\ B_{2m} \end{bmatrix}.$$

The boundary conditions are applied next, with impedances at the ends between the two wires and between each wire and ground. Additionally, each impedance to ground is in series with a voltage source. For a cable of length L, the boundary conditions are represented as

$$[V]_{x=0} = [X][V_s]+[C][I]_{x=0} \text{ and}$$

$$[V]_{x=L} = [W][V_L]+[D][I]_{x=L}$$

with

$[C]^{-1}$ - a 2x2 matrix with $C_{ii} = -\sum_j \frac{1}{Z_{s_{ij}}}$ and $C_{ij} = \frac{1}{Z_{s_{ij}}}$,

$[D]^{-1}$ - a 2x2 matrix with $D_{ii} = \sum_j \frac{1}{Z_{L_{ij}}}$ and $D_{ij} = \frac{-1}{Z_{L_{ij}}}$,

$[X]$ - a 2x2 matrix with $X_{ij} = -\frac{C_{ij}}{Z_{s_{jj}}}$,

$[W]$ - a 2x2 matrix with $W_{ij} = \frac{D_{ij}}{Z_{L_{jj}}}$,

$[V_s]$ - a 2x1 column matrix of voltage sources on one end of the cable,

$[V_L]$ - a 2x1 column matrix of voltage sources on the other end of the cable,

$Z_{s_{ij}}$ - the impedance between the i and j wires on one end of the cable,

and $Z_{L_{ij}}$ - the impedance between the i and j wires on the other end of the cable.

Finally, the remaining unknowns are determined as follows

$$\begin{bmatrix}[R]\\[S]\end{bmatrix} = \begin{bmatrix} [H] + \frac{1}{i\gamma}[C][Y] & [H] - \frac{1}{i\gamma}[C][Y] \\ e^{i\gamma L}([H] + \frac{1}{i\gamma}[D][Y]) & e^{-i\gamma L}([H] - \frac{1}{i\gamma}[D][Y]) \end{bmatrix}$$

$$\times \begin{bmatrix} [X][V_S] + [C]([\Sigma_m P_m] + [\Sigma_m Q_m]) - ([\Sigma_m M_m] + [\Sigma_m N_m]) \\ [W][V_L] + [D]([\Sigma_m P_m e^{i\alpha_m L}] + [\Sigma_m Q_m e^{i\beta_m L}]) - ([\Sigma_m M_m e^{i\alpha_m L}] + [\Sigma_m N_m e^{i\beta_m L}]) \end{bmatrix}$$

with

$$[H] = \begin{bmatrix} 1 & 0 \\ 0 & 1 \end{bmatrix}.$$

Even though the BTSP code is written to solve all these equations specifically for a BTSP cable, it is possible to extend it to more conductors, or to cables with multiple shields.

END

DATE
FILMED

07-82

DTIC